

Article

Microstructure Evolution and Mechanical Properties of Titanium/Alumina Brazed Joints for Medical Implants

Hong Bian ^{1,2,3}, Xiaoguo Song ^{1,2,3,*} , Shengpeng Hu ³ , Yuzhen Lei ³, Yide Jiao ³, Shutong Duan ³, Jicai Feng ^{1,2} and Weimin Long ⁴

¹ School of Materials Science and Engineering, Harbin Institute of Technology, Harbin 150001, China; whenstreaming163@163.com (H.B.); feng_jicai@163.com (J.F.)

² State Key Laboratory of Advanced Welding and Joining, Harbin Institute of Technology, Harbin 150001, China

³ Shandong Provincial Key Lab of Special Welding Technology, Harbin Institute of Technology at Weihai, Weihai 264209, China; husp@hitwh.edu.cn (S.H.); lei.yuzhen@163.com (Y.L.); harrisjiao@163.com (Y.J.); shutong0724@163.com (S.D.)

⁴ State Key Laboratory of Advanced Brazing Filler Metals and Technology, Zhengzhou Research Institute of Mechanical Engineering, Zhengzhou 450001, China; brazelong@163.com

* Correspondence: xgsong@hitwh.edu.cn; Tel./Fax: +86-631-5678454

Received: 7 May 2019; Accepted: 31 May 2019; Published: 3 June 2019



Abstract: Medical titanium and alumina (Al_2O_3) bioceramic are widely utilized as biomaterials. A reliable brazed joint of titanium and alumina was successfully obtained using biocompatible Au foil for implantable devices in the present study. The interfacial microstructure and reaction products of titanium/Au/ Al_2O_3 joints brazed under different conditions were investigated by scanning electron microscopy (SEM), energy dispersive spectroscopy (EDS), and X-ray diffraction (XRD). In this study, the typical interfacial microstructure of the titanium/Au/ Al_2O_3 joint was titanium/ Ti_3Au layer/ TiAu layer/ TiAu_2 layer/ TiAu_4 layer/Au + granular TiAu_4 layer/ TiO_x phase/ Al_2O_3 ceramic. With increasing brazing temperature or holding time, the thicknesses of Ti_3Au + TiAu + TiAu_2 layers adjacent to the titanium substrate increased gradually. Shear tests indicated that the joint brazed at 1115 °C for 3 min exhibited the highest shear strength of 39.2 MPa. Typical fracture analysis displayed that the crack started at the Al_2O_3 ceramic and propagated along the interface of TiAu_2 and TiAu_4 reaction layers.

Keywords: brazing; titanium; alumina; interfacial microstructure; mechanical properties

1. Introduction

Titanium and its alloys have been intensively investigated and applied for biomedical applications because of their excellent biocompatibilities, mechanical properties, and corrosion resistances [1–6]. Applications have included dental implants, craniomaxillofacial implants, implants for artificial joint replacement and spinal components, internal fixation plates and screws, and housings for ventricular-assist devices and pacemaker cases [7–9]. Alumina, a ceramic with outstanding physical, chemical, and mechanical performances, has attracted great interest in industrial applications such as biomaterials, aerospace, nuclear power, automobiles, and electronics [10–13]. With excellent advantages in chemical stability, wear resistance, and biocompatibility, alumina has been a preferable orthopedic implant material used in dental and bone replacements as well as coatings for metallic materials [9,14–16]. Utilization of metal–ceramic composites for biomedical applications, including implantable pacemakers, retinal implants, and microstimulators, has dramatically increased in recent

years [17]. To extend the practical utilization of metal–ceramic composite components, biocompatible metal–ceramic joints are desirable for implantable medical devices [17,18].

Nevertheless, ceramic–metal joints with sufficient mechanical integrity are difficult to achieve because of the large differences in physical and mechanical properties between ceramics and metals such as coefficient of thermal expansion (CTE), chemical composition, and modulus of elasticity (MOE) [10,19]. In the brazing of ceramics to metals, a main problem that needs to be solved is the poor wettability of liquid brazing alloy on ceramics. Active brazing is a promising approach that introduces active elements such as Ti, Zr, Ni, or V into brazing alloys [20–23], which significantly enhances wettability and spreading of liquid metal on ceramics by metallurgical bonding [24].

Ti is a typical active element that promotes wetting and adhesion. The interfacial reactions on the metal/alumina interface have been investigated using various Ti-containing metal alloys such as CuAg-Ti/alumina [21,25,26], AgCu-Ti/alumina [27,28], CuSn-Ti/alumina [29], NiPd-Ti/alumina [30], SnAgCu-Ti/alumina [31], and NiTiZr/alumina [24]. Voytovych et al. identified the existence of M_6X -type compounds and titanium oxides (TiO_x on a metal/ Al_2O_3 ceramic interface) whose chemical compositions were believed to be greatly dependent on the activity of Ti [25]. Decrease in the activity of Ti in the system leads to the formation of titanium oxides with higher oxidation on the interface, resulting in a higher final contact angle. Similar conclusions were made by Kritsalis et al. after studying an NiPd-Ti/alumina system [30].

It has been widely reported that alumina could be brazed to different metals with Ti-containing filler alloys [10,21,32–37]. The types of titanium oxides that form in an Al_2O_3 /Kovar joint using Ag-Pd/Ti filler are found to be affected by the thickness of the Ti layer, and the joint strengths are influenced by the thicknesses of the reaction layer and residual Ti layer [32]. Xin et al. investigated the reaction products on the Ti film/ Al_2O_3 interface for an Al_2O_3 /Kovar joint and suggested that a competitive reaction mechanism existed in the system. At temperatures lower than 1057 °C, Ti reacts with Al from the decomposition of Al_2O_3 , resulting in the formation of Ti_3Al . As the reaction proceeds, TiO precipitates out from a Ti solid solution as the O concentration rises above the solubility in Ti and Ti_3Al . For test temperatures higher than 1057 °C, Ti directly reacts with O from Al_2O_3 to generate TiO and Ti_3Al [10]. Simultaneously, the type of Ti oxide depends on the activity of Ti in the reaction layer, which could be decreased by the interaction between Ti and Ni from Kovar substrate to form Ni_3Ti , resulting in a shift of reaction product from TiO to Ti_2O_3 or Ti_3O_5 [35]. This is also observed by other investigations [38–40].

The other challenge in brazing ceramics to metals is the thermal stress generated on the metal–ceramic interface resulting from CTE mismatch between them as the joint cools to room temperature. The addition of pure gold, which is biocompatible, is desired because it can release thermal stresses by plastic deformation.

In this study, reliable brazing of Al_2O_3 ceramic to medical titanium alloy was achieved using pure gold foil. Detailed investigations on the effects of brazing temperature and dwelling time on microstructure evolution and mechanical properties were conducted. Mechanical properties were analyzed from microhardness data for different phases as well as shear strength of the joints.

2. Experimental Materials and Methods

Commercial polycrystalline Al_2O_3 ceramic with a purity of 99.5% (Shanghai Unite Technology Co., Ltd., Shanghai, China) was processed into 5 mm × 5 mm × 5 mm cubes. The dimensions of pure α -titanium (Kunshan Bitait Metal Products Co., Ltd., Kunshan, China) used herein were approximately 20 mm × 10 mm × 5 mm. Figure 1a shows the SEM image of Al_2O_3 in back-scattered electron (BSE) mode, and Figure 1b displays the metallograph of titanium, indicating the equiaxed structure of the α -Ti alloy. Au foil of purity 99.99% (KYKY Technology Co., Ltd., Beijing, China) with a thickness of 50 μ m was used.

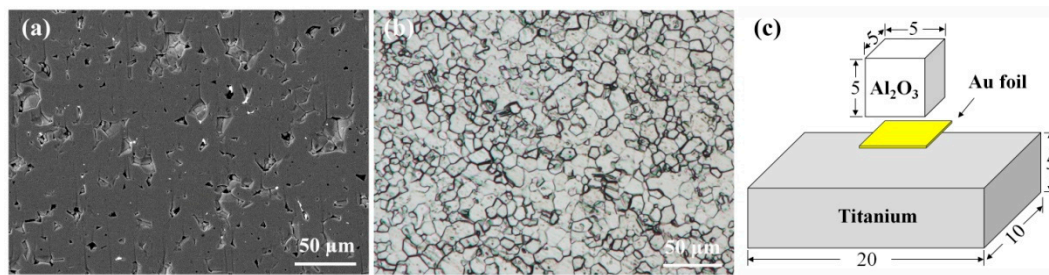


Figure 1. Microstructures of substrates and schematic diagram of brazing assembly. (a) BSE image of Al_2O_3 ceramic, (b) metallographic figure of α -Ti alloy, and (c) brazing assembly (mm).

To obtain titanium/Au/ Al_2O_3 brazed joints, the joining surface of titanium was ground to a grit of 3000 with emery paper. The Al_2O_3 ceramic, Au foil, and α -titanium were all cleaned with acetone in an ultrasonic bath for 15 min, and then they were assembled as a sandwich structure, as described in Figure 1c. The atmosphere of the vacuum furnace was maintained at 1.3×10^{-3} Pa during the brazing process. The furnace was firstly heated to 1000 °C for 10 min at a rate of 20 °C/min then to the brazing temperatures at a rate of 10 °C/min. Afterwards, in order to investigate the impact of brazing temperature on the microstructures and mechanical properties of the brazed joints, the brazing specimens were held for 1 min at different brazing temperatures. Finally, the specimens were cooled down to 300 °C at a rate of 5 °C/min and then to room temperature spontaneously in the furnace. To investigate the effect of holding time on the microstructures and mechanical properties of the brazed joints, the brazing specimens were kept for different holding times at 1115 °C. About 10 specimens were prepared in the same condition for each parameter.

The cross-sections of titanium/Au/ Al_2O_3 brazed joints were characterized using SEM (MERLIN Compact, ZEISS, Stuttgart, Germany) equipped with an energy-dispersive X-ray spectrometer (EDS, Octane Plus, EDAX, Mahwah, NJ, USA). Shear tests were conducted on at least six specimens at room temperature at a constant strain rate of 1 mm/min using a universal testing machine (Instron 5967, Instron, Boston, MA, USA). Average values and deviations of shear strengths were calculated from five specimens after removing outliers for each parameter. After the shear test, the fractures of titanium/Au/ Al_2O_3 brazed joints were analyzed by three fractured specimens selected randomly using SEM and X-ray diffraction (XRD, JDX-3530M). To further evaluate mechanical properties of the reaction products in the joint, the hardness and elastic modulus across the joints were measured using a nanoindenter (G200, Agilent, Santa Clara, CA, USA).

3. Results and Discussion

3.1. Typical Interfacial Microstructure of the Titanium/Au/ Al_2O_3 Joint

Vacuum brazing of titanium alloy and Al_2O_3 ceramic was achieved using Au filler foil. Figure 2 shows the typical interfacial microstructure and the main element distribution of the titanium/Au/ Al_2O_3 joint brazed at 1115 °C for 1 min. As shown in Figure 2a, according to the different contrasts of each phase by SEM in the backscattered electron mode, the joint could be classified into four continuous reaction zones (zone I to IV), and zone V adjacent to the Al_2O_3 substrate consisted of a white phase dispersed with some light grey granular phases.

Figure 2a also shows variations of elemental concentration of Ti, Au, Al, and O along the white dashed line. The concentration profile of element Ti showed a stepwise decrease from titanium substrate to Al_2O_3 ceramic, with a noticeable enrichment on the metal/ Al_2O_3 interface. Meanwhile, the main distribution of element Au in the seam exhibited a stepwise increase from titanium to Al_2O_3 ceramic, and it displayed a minute amount in titanium substrate. The elements of Al and O were mainly distributed in Al_2O_3 ceramic. These results were consistent with the corresponding elemental distribution in the typical joint displayed in Figure 2b–e.

The interdiffusion of Ti and Au indicated that the active element Ti diffused from the titanium substrate and spread in the brazing seam, and it eventually accumulated adjacent to the surface of Al_2O_3 ceramic. Meanwhile, Au melted and diffused into the titanium substrate during the brazing process.

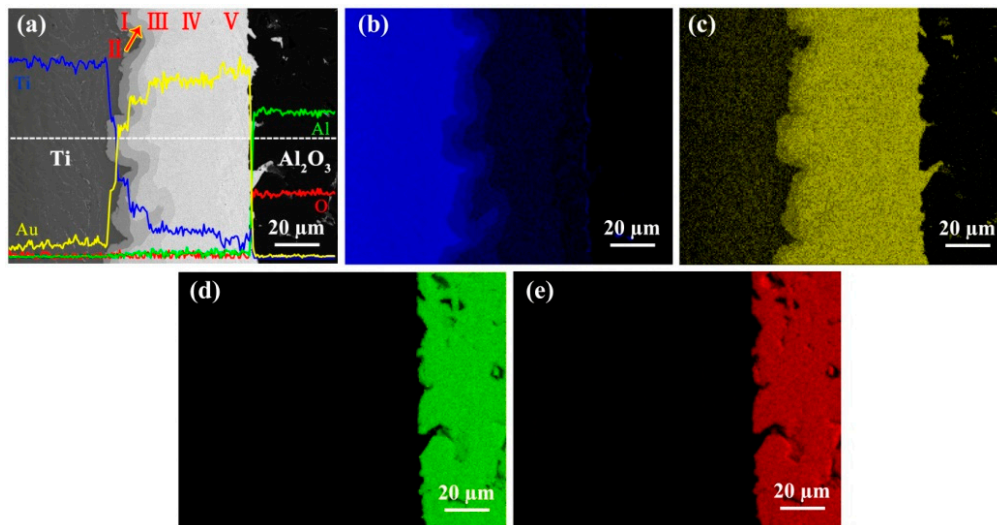


Figure 2. Microstructure and corresponding element distribution of the titanium/Au/ Al_2O_3 joint brazed at $1115\text{ }^\circ\text{C}$ for 1 min. (a) Microstructure and elemental distribution maps of (b) Ti, (c) Au, (d) Al, and (e) O.

In order to investigate microstructure characteristics of the titanium/Au/ Al_2O_3 joint in detail, Figure 3 shows the microstructures of zones I–V under high magnification. EDS data showing elemental concentrations and possible phases at each spot are listed in Table 1. The characteristic areas of I to VI adjacent to titanium are shown in Figure 3a under high magnification. The characteristic areas of VI and V next to Al_2O_3 ceramic are displayed in Figure 3b under high magnification. According to the EDS results shown in Table 1 and the Ti–Au binary phase diagram illustrated in Figure 4 [41], the reaction layers that formed from the titanium substrate to Al_2O_3 substrate were a Ti_3Au phase (Spot A), a TiAu phase (Spot B), a TiAu₂ phase (Spot C), a TiAu₄ phase (Spot D), and an Au phase (Spot E) containing TiAu₄ particles, respectively.

From the above analysis, it was proposed that during brazing, active element Ti spread and accumulated on the metal/ Al_2O_3 ceramic interface, which could be deduced from the reaction with Al_2O_3 and the formation of TiO_x [25,30,31,42,43]. However, TiO_x was hard to observe with SEM and EDS owing to its limited thickness. Apart from reacting with Al_2O_3 , the dissolved Ti in the brazing seam also reacted with molten Au, forming Ti–Au intermetallic compounds (IMCs).

To sum up, the typical interfacial microstructure of the titanium/Au/ Al_2O_3 joint brazed at $1115\text{ }^\circ\text{C}$ for 1 min consisted of titanium/ Ti_3Au layer/TiAu layer/TiAu₂ layer/TiAu₄ layer/Au + granular TiAu₄ layer/ TiO_x phase/ Al_2O_3 ceramic.

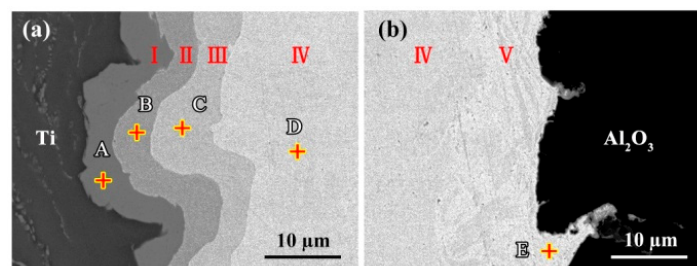
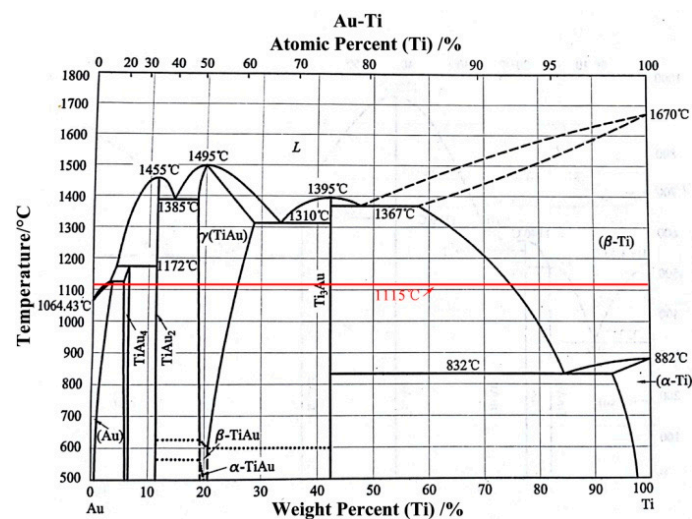


Figure 3. Microstructure of the titanium/Au/ Al_2O_3 joint at a high magnification: (a) the titanium/brazing seam interface; (b) the brazing seam/ Al_2O_3 interface.

Table 1. Energy dispersive spectroscopy (EDS) results of the spots marked in Figure 3 (at. %).

Spot	Ti	Au	Al	O	Possible Phase
A	72.64	23.63	0.02	3.71	Ti ₃ Au
B	48.44	45.89	0.06	5.61	TiAu
C	32.80	63.14	0.03	4.03	TiAu ₂
D	18.44	73.80	0.04	7.72	TiAu ₄
E	3.38	86.15	0.56	9.91	Au

In order to illuminate the formation mechanism of the typical interfacial microstructure and different Ti–Au IMCs in the titanium/Au/Al₂O₃ joint, the Ti–Au binary system was studied using the phase diagram shown in Figure 4 [41]. The complex interfacial microstructural morphology and arrangement of various intermetallic compounds (IMCs) generated during the brazing process were strongly dependent on the brazing temperature. The brazing process of titanium to Al₂O₃ ceramic can be deduced as follows. According to the Ti–Au binary phase diagram (Figure 4), it was observed that element Au melted to the liquid phase when the temperature exceeded 1064 °C. The active element Ti diffused from titanium substrate and dissolved into liquid Au gradually. As shown in Figure 4, marked by the red line at 1115 °C, with an increasing Ti concentration in the liquid phase, Ti began to react with molten Au to form TiAu₄ IMC by the peritectic reaction of Au(L) + Ti → TiAu₄. Thus, a continuous TiAu₄ layer formed in the brazing seam and inhibited the interdiffusion of Ti and Au. Because of the decreasing concentration gradient of Ti from titanium to the TiAu₄ layer, the Ti₃Au, TiAu, and TiAu₂ layers simultaneously formed between titanium and the TiAu₄ layer. During the cooling process, TiAu₄ particles and the Au phase directly precipitated in the remnant liquid phase by the eutectic reaction of L → Au + TiAu₄ adjacent to the ceramic substrate. Finally, the typical microstructure of titanium/Au/Al₂O₃ joint with five reaction zones was obtained in the brazing seam, as illustrated in Figure 3.

**Figure 4.** Ti–Au binary phase diagram.

3.2. Effects of Processing Parameters on the Microstructure of the Titanium/Au/Al₂O₃ Joint

Figure 5 displays the microstructure evolution of the joints brazed at different temperatures for 1 min. Brazing temperatures had a significant effect on the interfacial microstructure, and the thicknesses of reaction layers were measured and illustrated in Figure 5f. With increasing temperature, the thicknesses of Ti₃Au + TiAu + TiAu₂ layers (zone I–III) adjacent to the titanium substrate increased gradually (Figure 5a–e). The thickness of the TiAu₂ layer (zone III) increased first and then decreased, and the maximum thickness of 17.4 μm was obtained under 1115 °C. Meanwhile, as the brazing

temperature increased, the thickness of the Au layer with granular TiAu_4 (zone V) next to Al_2O_3 ceramic notably decreased.

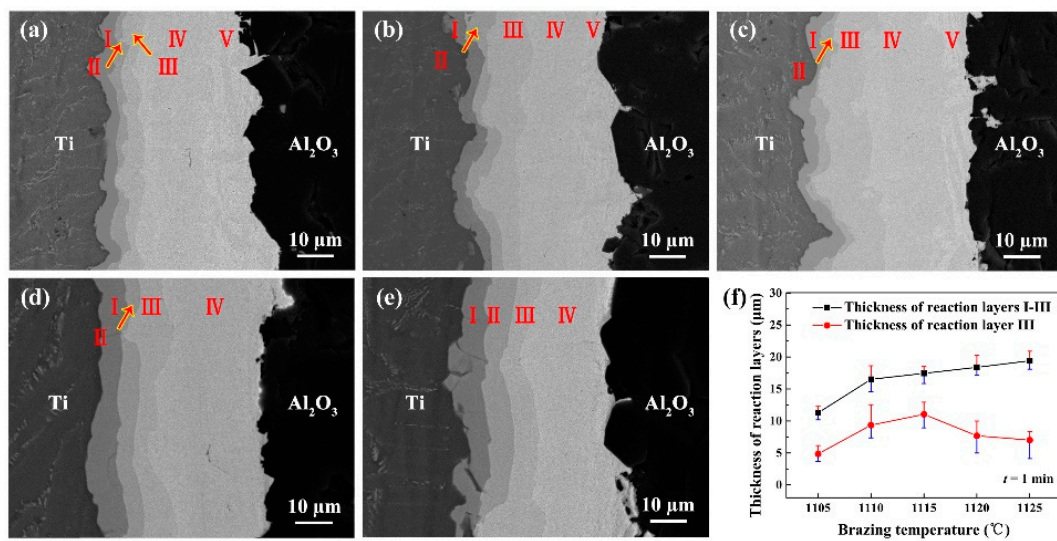


Figure 5. Microstructure of the titanium/Au/ Al_2O_3 joint brazed at different brazing temperature for 1 min: (a) 1105 °C, (b) 1110 °C, (c) 1115 °C, (d) 1120 °C, (e) 1125 °C, and (f) the thicknesses of Ti-Au layers (zone I-III).

Figure 6 shows the microstructure evolution of the joints brazed at 1115 °C for different holding times. The microstructure of the joints changed significantly with the prolongation of holding time, and the thickness of the reaction layers were measured and illustrated in Figure 6d. As shown in Figure 6a–c, with the prolongation of holding time from 1 to 5 min, the thicknesses of $\text{Ti}_3\text{Au} + \text{TiAu} + \text{TiAu}_2$ layers (zone I-III) increased. The thickness of the TiAu_2 layer (zone III) increased first and then decreased, and the maximum thickness was obtained for a holding time of 3 min. Meanwhile, as the holding time increased, the thickness of the Au layer with granular TiAu_4 (zone V) next to Al_2O_3 ceramic did not change significantly.

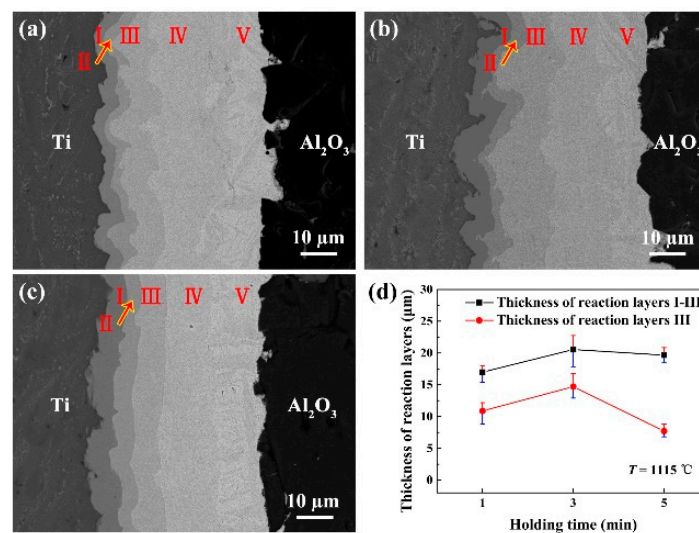


Figure 6. Microstructure of the titanium/Au/ Al_2O_3 joint brazed at 1115 °C for different holding times: (a) 1 min, (b) 3 min, (c) 5 min, and (d) the thicknesses of Ti-Au layers (zone I-III).

Based on the above analyses, brazing temperature and holding time, which affected the dissolution of Ti from titanium substrate, had significant effects on the microstructure evolution of the joints.

A conceptual model was established and illustrated in Figure 7 to show the evolution of the microstructure. The reaction process could be classified into three stages. As shown in Figure 7a, during the brazing process when the temperature was above the melting point of Au, Au foil first converted into liquid. Then, Ti dissolved into molten Au under the driving force of the concentration gradient, and it reacted with Au to form the TiAu₄ layer between the Ti substrate and Au (Figure 7b). Finally, the Ti₃Au, TiAu, and TiAu₂ layers simultaneously formed between titanium and the TiAu₄ layer along the concentration gradient of Ti. During the cooling process, TiAu₄ particles and the Au phase directly precipitated because the residual element Ti was present in the remnant liquid phase adjacent to the ceramic substrate (Figure 7c). When brazing temperature or holding time increased, the mutual diffusion of Ti and Au became more sufficient. As a result, the thicknesses of Ti₃Au + TiAu + TiAu₂ layers increased gradually, especially the TiAu₂ layer. Meanwhile, the Au phase containing TiAu₄ particles reduced, as shown in Figure 7d. With the further increase of brazing temperature or holding time, the diffusion of Au was adequate, and the amount of Ti was sufficient. Ti₃Au and TiAu layers increased, resulting in the decreased thickness of the TiAu₂ layer. It was notable that the TiAu₄ layer almost occupied the brazing seam next to the ceramic (Figure 7e).

It has been widely reported that TiO_x could be generated on the interface of Ti containing metal and Al₂O₃ [25,30,32,35,38–40]. The limited thickness of TiO_x and many other compounds in metal–ceramic interfaces led to a decreased accuracy in the identification of titanium oxides [20,44]. As brazing temperature or holding time rose, more TiO_x phases formed adjacent to Al₂O₃ (Figure 7c–e).

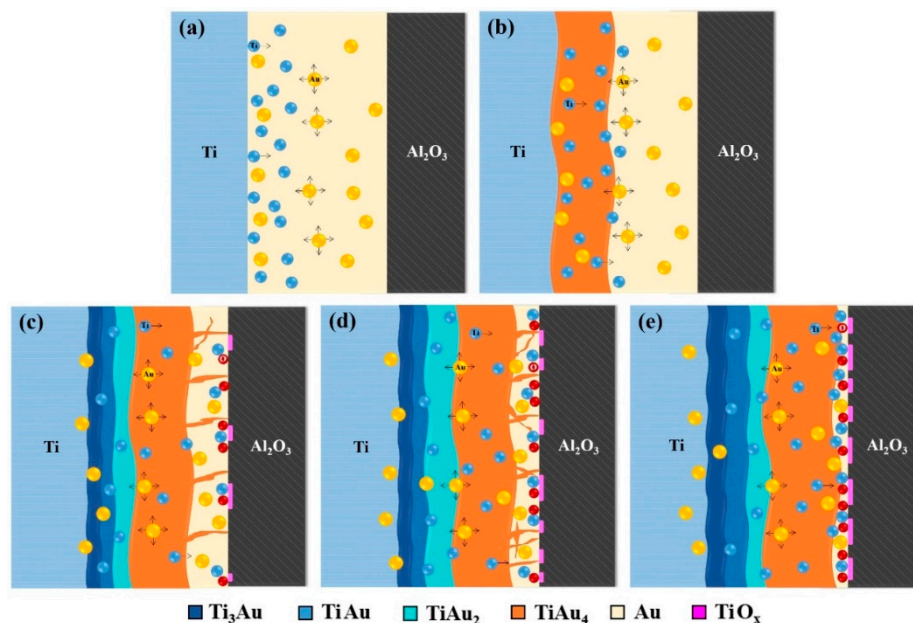


Figure 7. Schematic of the microstructure evolution for the titanium/Au/Al₂O₃ joint. (a) Mutual diffusion of Ti and Au; (b) formation of the TiAu₄ layer; (c) formation of reaction layers of the joint; and (d) and (e) growth of reaction layers with the increase of brazing temperature or holding time.

3.3. Mechanical Properties and Fracture Morphology of Titanium/Au/Al₂O₃ Joints

In order to evaluate the effect of brazing temperature and holding time on the mechanical properties of brazed joints, the shear strength of the joints was tested at room temperature, as shown in Figure 8. As shown in Figure 8a, when the joints were brazed at different temperatures varying from 1105 to 1125 °C for 1 min, the shear strength of the joints increased first and then decreased. The maximum average shear strength of 20.3 MPa was obtained when the joints were brazed at 1105 °C for 1 min.

As shown in Figure 8b, the shear strength of the joints firstly increased and then decreased when the joints were brazed at 1115 °C for different holding times prolonged from 1 to 5 min. The maximum

value of shear strength reached 39.2 MPa when the holding time was 3 min, which was about twice that of the joints brazed at 1115 °C for 1 min.

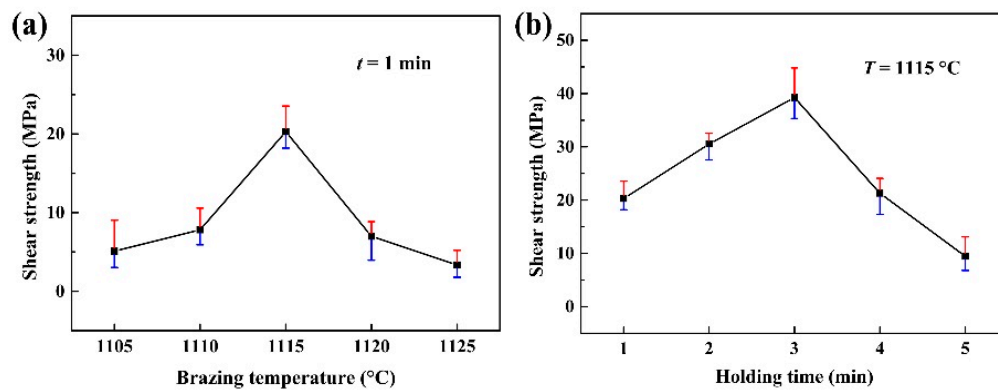


Figure 8. Effect of (a) brazing temperature and (b) holding time on shear strength of titanium/Au/Al₂O₃ joints.

Fracture analysis was conducted using an optical microscope, SEM, and XRD to investigate the fracture location and fracture path of the titanium/Au/Al₂O₃ joints brazed at 1115 °C for 1 min. As shown in Figure 9a,b, Al₂O₃ ceramic was observed on the fracture surface of the titanium side. Figure 9d shows the crack was initiated at the Al₂O₃ ceramic and propagated into the brazing seam via the Au/Al₂O₃ interface during the shear test. The magnified SEM image of Figure 9d is shown in Figure 9e. When the crack propagated into the brazing seam, the joints fractured along the interface of TiAu₂ and TiAu₄ reaction layers (the interface of zone III and zone IV). The joints brazed at 1115 °C for 1 min fractured in the brittle mode. To further investigate the fracture location, reaction phases on the fracture surface of the titanium side were identified using XRD analysis, as shown in Figure 9c. It was evident that the fracture surface of the titanium side consisted of Au, Al₂O₃, and TiAu₂, which corresponded to the fracture path analyses of Figure 9d,e.

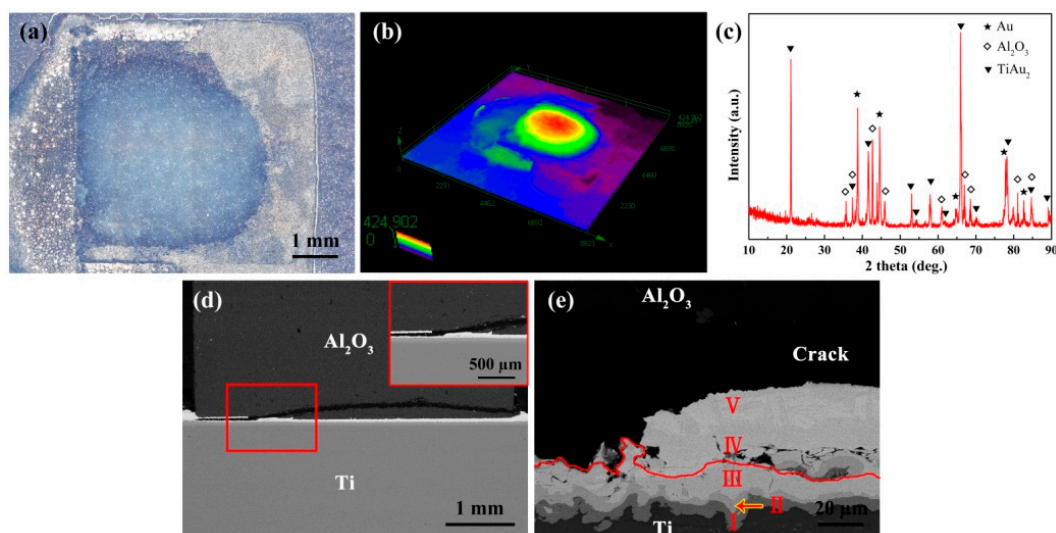


Figure 9. Fracture analysis of titanium/Au/Al₂O₃ joints brazed at 1115 °C for 1 min after the shear test. (a) Fracture surface of Ti alloy side, (b) 3D image of (a), (c) XRD pattern of (a), (d) fracture path of the Ti/Au/Al₂O₃ joint, and (e) high-magnification image of (d).

Figure 10 displays the fracture analyses of the joints brazed at different parameters. It was observed that two types of fracture patterns existed after the shear test. In the first fracture pattern, significantly flat fracture surfaces were clearly observed, and the joints fractured along the Au/Al₂O₃

interface during the shear tests when brazed at 1105 °C for 1 min and 1115 °C for 5 min (Figures 9c and 10a). XRD analyses of the fracture surface on the titanium side displayed detectable phases, including Au and Al₂O₃, which in turn supported the above analysis of the first fracture pattern. Meanwhile, as shown in Figure 10b, a second type of fracture pattern was observed when the joints were brazed at 1115 °C for 3 min, identical with that brazed at 1115 °C for 1 min. In the second type, the fracture started at the Al₂O₃ ceramic and propagated along the interface of TiAu₂ and TiAu₄ reaction layers, which was confirmed by the existence of Au, Al₂O₃, and TiAu₂ in the XRD result.

Variations in shear strength were significant count on the microstructure evolution of the joint. The increase of brazing temperature and holding time can promote the diffusion of active Ti from the titanium substrate and aggregation adjacent to Al₂O₃ ceramic. When the brazing temperature was lower (or the holding time was shorter), the diffusions of Ti and Au were limited, and the reaction layer of TiO_x was extremely thin as the weakest position of the bonding. Therefore, the shear strength of the joints was quite low, and the joint fractured along the Au/Al₂O₃ interface. With the increase of brazing temperature (or the prolongation of holding time), the TiO_x layer thickened, which could improve the metallurgical bonding between brazing alloy and ceramic. Therefore, the shear strength of the joints increased. Fractures occurred at the Au/Al₂O₃ interface and fragile Ti–Au reaction layers. When the brazing temperature further increased (or holding time was further prolonged), there was a drop in shear strength, which could be attributed to two factors: the over-thickened TiO_x layer and the higher stresses resulting from the increased temperature or changed microstructure of Ti–Au IMCs layers in the brazing seam. Based on the above analyses, it can be concluded that a suitable thickness of the TiO_x layer adjacent to ceramic had crucial influence on the shear strength of the joints.

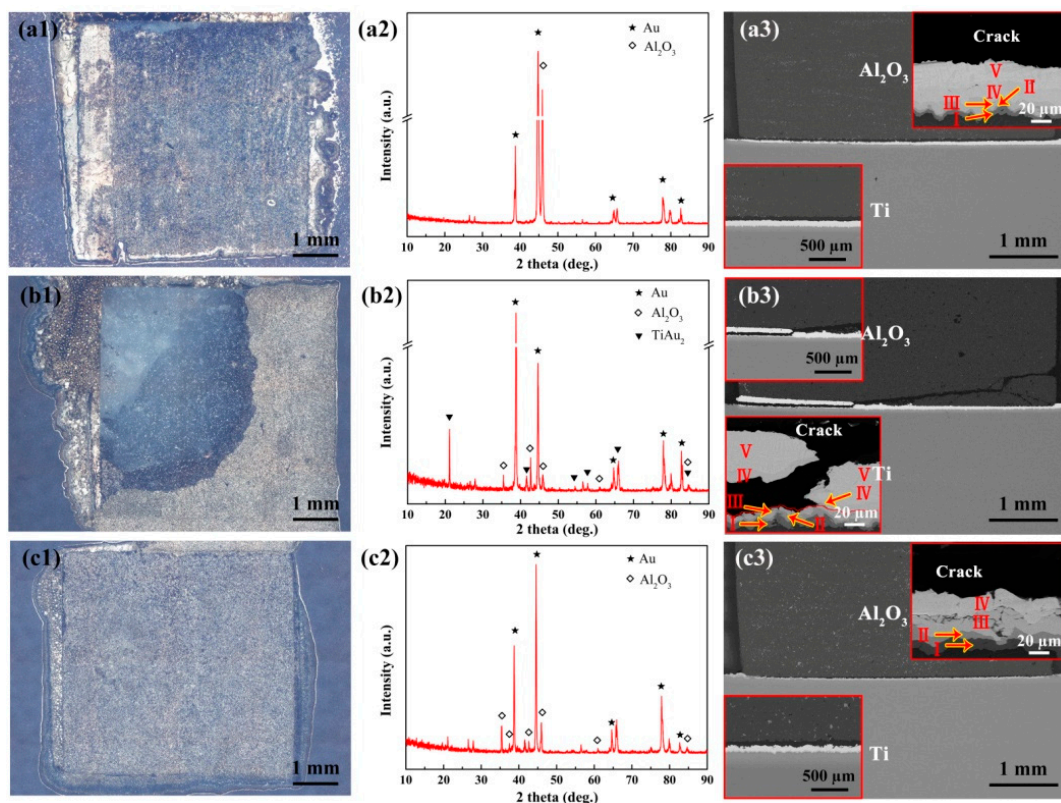


Figure 10. Fractographs and XRD patterns of titanium/Au/Al₂O₃ joints brazed at different parameters after the shear test. (a1–a3) 1105 °C for 1 min, (b1–b3) 1115 °C for 3 min, and (c1–c3) 1115 °C for 5 min.

Figure 11 shows nanoindentation test results, which displayed the variation in hardness and elastic modulus of reaction phases for the joint brazed at 1115 °C for 3 min. As shown in Figure 11a, the highest hardness (9.9 GPa) and elastic modulus (165.0 GPa) across the joint was found in the Ti₃Au

layer, while the Au phase showed the lowest hardness (2.7 GPa) and elastic modulus (115.0 GPa). In order to reveal elastic and plastic behaviors of reaction phases across the joint, typical loads versus depth curves are illustrate in Figure 11b. The deformation process of reaction phases could be divided into elastic-plastic loading and purely elastic unloading. It was apparent that the Au phase possessed the lowest elastic recovery of 14.1%, which recovered 69 nm of the total indentation depth (488 nm). These results showed that the deformation behavior of the Au phase was primarily plastic compared to other phases, which could be beneficial to release residual stress caused by CTE mismatch.

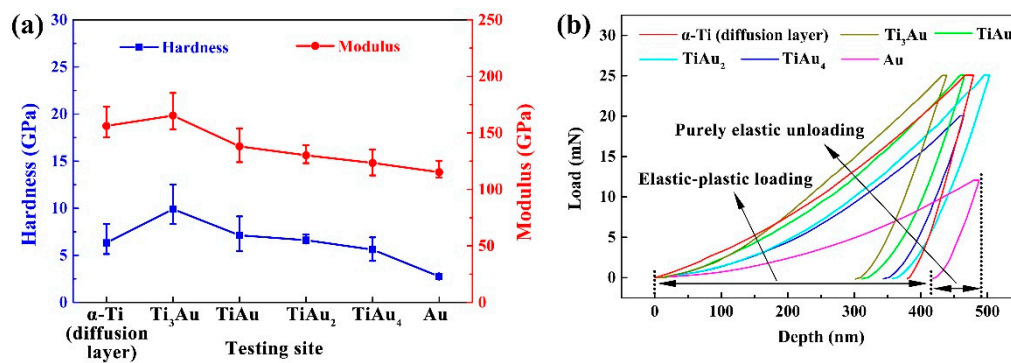


Figure 11. (a) Hardness and elastic modulus distribution across the joint interface; (b) typical load versus depth curves.

4. Conclusions

In this study, a reliable brazing joint of medical titanium and alumina bioceramic was successfully obtained using Au foil. The microstructure, reaction products, and shear strength of titanium/Au/ Al_2O_3 joints were studied. The conclusions are summarized as follows:

- (1) The typical interfacial microstructure of the titanium/Au/ Al_2O_3 joint was titanium/ Ti_3Au layer/ $TiAu$ layer/ $TiAu_2$ layer/ $TiAu_4$ layer/Au + granular $TiAu_4$ layer/ TiO_x phase/ Al_2O_3 ceramic.
- (2) Brazing temperature displayed significant effects on the microstructure evolution and mechanical properties of brazed joints. With the increase of brazing temperature, the mutual diffusion of Ti and Au was enhanced, and the thickness of Ti_3Au + $TiAu$ + $TiAu_2$ layers adjacent to the titanium substrate increased gradually. Meanwhile, the thickness of the Au layer with granular $TiAu_4$ next to Al_2O_3 ceramic notably decreased. The TiO_x phase, which promoted metallurgical bonding between the brazing alloy and Al_2O_3 ceramic, could increase as more Ti reacts with Al_2O_3 . The shear strength of the joints increased first and then decreased. When the brazing temperature was 1115 °C, a maximum shear strength was obtained as a result of the TiO_x layer with a suitable thickness. Similar effects of holding time on microstructure evolution and mechanical properties were also observed, and the maximum shear strength was obtained for a holding time of 3 min.
- (3) Shear tests indicated that the joint brazed at 1115 °C for 3 min exhibited the highest shear strength of 39.2 MPa. Typical fracture analysis displayed that the crack started at the Al_2O_3 ceramic and propagated along the interface of $TiAu_2$ and $TiAu_4$ reaction layers.

Author Contributions: Conceptualization, X.S. and W.L.; Formal analysis, H.B.; Investigation, H.B. and S.D.; Project administration, J.F.; Resources, Y.L.; Supervision, X.S.; Validation, S.H.; Visualization, Y.J.; Writing—original draft and revising, H.B.; Writing—review and editing, all the authors; Writing—revising, S.H. and W.L.

Funding: This project is supported by the National Natural Science Foundation of China (Grant Nos. 51775138, U1537206 and U1737205), and the Key Research & Development program of Shandong Province (No. 2017GGX40103).

Conflicts of Interest: The authors declare no conflict of interest.

References

1. Geetha, M.; Singh, A.; Asokamani, R.; Gogia, A. Ti based biomaterials, the ultimate choice for orthopaedic implants—A review. *Prog. Mater. Sci.* **2009**, *54*, 397–425. [[CrossRef](#)]
2. Li, L.-H.; Kong, Y.-M.; Kim, H.-W.; Kim, Y.-W.; Kim, H.-E.; Heo, S.-J.; Koak, J.-Y. Improved biological performance of Ti implants due to surface modification by micro-arc oxidation. *Biomaterials* **2004**, *25*, 2867–2875. [[CrossRef](#)] [[PubMed](#)]
3. Symietz, C.; Lehmann, E.; Gildenhaar, R.; Krüger, J.; Berger, G. Femtosecond laser induced fixation of calcium alkali phosphate ceramics on titanium alloy bone implant material. *Acta Biomater.* **2010**, *6*, 3318–3324. [[CrossRef](#)] [[PubMed](#)]
4. Shukla, A.; Balasubramaniam, R.; Shukla, A. Effect of surface treatment on electrochemical behavior of CP Ti, Ti–6Al–4V and Ti–13Nb–13Zr alloys in simulated human body fluid. *Corros. Sci.* **2006**, *48*, 1696–1720. [[CrossRef](#)]
5. Ozdemir, Z.; Ozdemir, A.; Basim, G. Application of chemical mechanical polishing process on titanium based implants. *Mater. Sci. Eng. C* **2016**, *68*, 383–396. [[CrossRef](#)] [[PubMed](#)]
6. Revathi, A.; Borrás, A.D.; Muñoz, A.I.; Richard, C.; Manivasagam, G. Degradation mechanisms and future challenges of titanium and its alloys for dental implant applications in oral environment. *Mater. Sci. Eng. C* **2017**, *76*, 1354–1368. [[CrossRef](#)] [[PubMed](#)]
7. Chen, Q.; Thouas, G.A. Metallic implant biomaterials. *Adv. Mater. Sci. Eng. R. Rep.* **2015**, *87*, 1–57. [[CrossRef](#)]
8. Hussein, M.A.; Kumar, M.; Drew, R.; Al-Aqeeli, N. Electrochemical corrosion and in vitro bioactivity of nano-grained biomedical Ti-20Nb-13Zr alloy in a simulated body fluid. *Materials* **2018**, *11*, 26. [[CrossRef](#)]
9. Weng, Y.; Liu, H.; Ji, S.; Huang, Q.; Wu, H.; Li, Z.; Wu, Z.; Wang, H.; Tong, L.; Fu, R.K.; et al. A promising orthopedic implant material with enhanced osteogenic and antibacterial activity: Al₂O₃-coated aluminum alloy. *Appl. Surf. Sci.* **2018**, *457*, 1025–1034. [[CrossRef](#)]
10. Xin, C.; Liu, W.; Li, N.; Yan, J.; Shi, S.-Q. Metallization of Al₂O₃ ceramic by magnetron sputtering Ti/Mo bilayer thin films for robust brazing to Kovar alloy. *Ceram. Int.* **2016**, *42*, 9599–9604. [[CrossRef](#)]
11. Kar, A.; Mandal, S.; Venkateswarlu, K.; Ray, A.K. Characterization of interface of Al₂O₃-304 stainless steel braze joint. *Mater. Charact.* **2007**, *58*, 555–562. [[CrossRef](#)]
12. Li, J.; Pan, W.; Yuan, Z.; Chen, Y. Titanium metallization of alumina ceramics by molten salt reaction. *Appl. Surf. Sci.* **2008**, *254*, 4584–4590. [[CrossRef](#)]
13. Sakka, S.; Bouaziz, J.; Ben Ayed, F. Sintering and mechanical properties of the alumina–tricalcium phosphate–titania composites. *Mater. Sci. Eng. C* **2014**, *40*, 92–101. [[CrossRef](#)] [[PubMed](#)]
14. Smargiassi, A.; Bertacchini, J.; Checchi, M.; Cavani, F.; Ferretti, M.; Palumbo, C. Biocompatibility Analyses of Al₂O₃-Treated Titanium Plates Tested with Osteocyte and Fibroblast Cell Lines. *Biomedicines* **2017**, *5*, 32. [[CrossRef](#)] [[PubMed](#)]
15. Zhao, J.; Pan, N.; Huang, F.; Aldarouish, M.; Wen, Z.; Gao, R.; Zhang, Y.; Hu, H.-M.; Shen, Y.; Wang, L.-X. Vx3-Functionalized Alumina Nanoparticles Assisted Enrichment of Ubiquitinated Proteins from Cancer Cells for Enhanced Cancer Immunotherapy. *Bioconjug. Chem.* **2018**, *29*, 786–794. [[CrossRef](#)] [[PubMed](#)]
16. Chevalier, J.; Gremillard, L. Ceramics for medical applications: A picture for the next 20 years. *J. Eur. Ceram. Soc.* **2009**, *29*, 1245–1255. [[CrossRef](#)]
17. Jiang, G.; Mishler, D.; Davis, R.; Mobley, J.P.; Schulman, J.H. Zirconia to Ti-6Al-4V braze joint for implantable biomedical device. *J. Biomed. Mater. Part B Appl. Biomater.* **2005**, *72*, 316–321. [[CrossRef](#)]
18. Peytour, C.; Berthet, P.; Barbier, F.; Revcolevschi, A. Interface microstructure and mechanical behaviour of brazed TA6V/zirconia joints. *J. Mater. Sci. Lett.* **1990**, *9*, 1129–1131. [[CrossRef](#)]
19. Park, J.-W.; Mendez, P.F.; Eagar, T.W. Strain energy release in ceramic-to-metal joints by ductile metal interlayers. *Scr. Mater.* **2005**, *53*, 857–861. [[CrossRef](#)]
20. Bian, H.; Fu, W.; Lei, Y.; Song, X.; Liu, D.; Cao, J.; Feng, J. Wetting and low temperature bonding of zirconia metallized with Sn_{0.3}Ag_{0.7}Cu-Ti alloys. *Ceram. Int.* **2018**, *44*, 11456–11465.
21. Kozlova, O.; Braccini, M.; Voytovych, R.; Eustathopoulos, N.; Martinetti, P.; Devismes, M.-F. Brazing copper to alumina using reactive CuAgTi alloys. *Acta Mater.* **2010**, *58*, 1252–1260. [[CrossRef](#)]
22. Xiong, H.-P.; Chen, B.; Pan, Y.; Zhao, H.-S.; Mao, W.; Cheng, Y.-Y. A Cu-Pd-V System Filler Alloy for Silicon Nitride Ceramic Joining and the Interfacial Reactions. *J. Am. Ceram. Soc.* **2014**, *97*, 2447–2454. [[CrossRef](#)]

23. Wang, H.; Cao, J.; Feng, J. Brazing mechanism and infiltration strengthening of CC composites to TiAl alloys joint. *Scr. Mater.* **2010**, *63*, 859–862. [[CrossRef](#)]
24. Siegmund, P.; Guhl, C.; Schmidt, E.; Roßberg, A.; Rettenmayr, M. Reactive wetting of alumina by Ti-rich Ni–Ti–Zr alloys. *J. Mater. Sci.* **2016**, *51*, 3693–3700. [[CrossRef](#)]
25. Voytovych, R.; Robaut, F.; Eustathopoulos, N. The relation between wetting and interfacial chemistry in the CuAgTi/alumina system. *Acta Mater.* **2006**, *54*, 2205–2214. [[CrossRef](#)]
26. Kozlova, O.; Voytovych, R.; Eustathopoulos, N. Initial stages of wetting of alumina by reactive CuAgTi alloys. *Scr. Mater.* **2011**, *65*, 13–16. [[CrossRef](#)]
27. Ali, M.; Knowles, K.M.; Mallinson, P.M.; Fernie, J.A. Interfacial reactions between sapphire and Ag–Cu–Ti-based active braze alloys. *Acta Mater.* **2016**, *103*, 859–869. [[CrossRef](#)]
28. Liu, X.; Zhang, L.; Sun, Z.; Feng, J. Microstructure and mechanical properties of transparent alumina and TiAl alloy joints brazed using Ag–Cu–Ti filler metal. *Vacuum* **2018**, *151*, 80–89. [[CrossRef](#)]
29. Lin, C.-C.; Chen, R.-B.; Shiue, R.-K. A wettability study of Cu/Sn/Ti active braze alloys on alumina. *J. Mater. Sci.* **2001**, *36*, 2145–2150. [[CrossRef](#)]
30. Kritsalis, P.; Drevet, B.; Valignat, N.; Eustathopoulos, N. Wetting transitions in reactive metal/oxide systems. *Scr. Metall. Mater.* **1994**, *30*, 1127–1132. [[CrossRef](#)]
31. Kang, J.R.; Song, X.G.; Hu, S.P.; Liu, D.; Guo, W.J.; Cao, J.; Fu, W. Wetting and Brazing of Alumina by Sn_{0.3}Ag_{0.7}Cu–Ti Alloy. *Met. Mater. Trans. A* **2017**, *48*, 5870–5878. [[CrossRef](#)]
32. Zhu, W.; Chen, J.; Jiang, C.; Hao, C.; Zhang, J. Effects of Ti thickness on microstructure and mechanical properties of alumina–Kovar joints brazed with Ag–Pd/Ti filler. *Ceram. Int.* **2014**, *40*, 5699–5705. [[CrossRef](#)]
33. Fu, W.; Song, X.; Hu, S.; Chai, J.; Feng, J.; Wang, G. Brazing copper and alumina metallized with Ti-containing Sn_{0.3}Ag_{0.7}Cu metal powder. *Mater. Des.* **2015**, *87*, 579–585.
34. Cao, Y.; Yan, J.; Li, N.; Zheng, Y.; Xin, C. Effects of brazing temperature on microstructure and mechanical performance of Al₂O₃/AgCuTi/Fe–Ni–Co brazed joints. *J. Alloy. Compd.* **2015**, *650*, 30–36. [[CrossRef](#)]
35. Xin, C.; Yan, J.; Li, N.; Liu, W.; Du, J.; Cao, Y.; Shi, H. Microstructural evolution during the brazing of Al₂O₃ ceramic to kovar alloy by sputtering Ti/Mo films on the ceramic surface. *Ceram. Int.* **2016**, *42*, 12586–12593. [[CrossRef](#)]
36. Niu, G.; Wang, D.; Yang, Z.; Wang, Y. Microstructure and mechanical properties of Al₂O₃/TiAl joints brazed with B powders reinforced Ag–Cu–Ti based composite fillers. *Ceram. Int.* **2017**, *43*, 439–450. [[CrossRef](#)]
37. Valette, C.; Devismes, M.-F.; Voytovych, R.; Eustathopoulos, N. Interfacial reactions in alumina/CuAgTi braze/CuNi system. *Scr. Mater.* **2005**, *52*, 1–6. [[CrossRef](#)]
38. Selverian, J.H.; Ohuchi, F.S.; Bortz, M.; Notis, M.R. Interface reactions between titanium thin films and (1–1 2) sapphire substrates. *J. Mater. Sci.* **1991**, *26*, 6300–6308. [[CrossRef](#)]
39. Meir, S.; Kalabukhov, S.; Frage, N.; Hayun, S. Mechanical properties of Al₂O₃/Ti composites fabricated by spark plasma sintering. *Ceram. Int.* **2015**, *41*, 4637–4643. [[CrossRef](#)]
40. Hayun, S.; Meir, S.; Kalabukhov, S.; Frage, N.; Zaretsky, E.; Subhash, G. Phase constitution and dynamic properties of spark plasma-sintered alumina-titanium composites. *J. Am. Ceram. Soc.* **2019**, *99*, 573–580. [[CrossRef](#)]
41. Murray, J.L. The Au–Ti (Gold–Titanium) system. *Bull. Alloy Phase Diagr.* **1983**, *4*, 278–283. [[CrossRef](#)]
42. Kar, A.; Mandal, S.; Ghosh, R.N.; Ghosh, T.K.; Ray, A.K. Role of Ti diffusion on the formation of phases in the Al₂O₃–Al₂O₃ brazed interface. *J. Mater. Sci.* **2007**, *42*, 5556–5561. [[CrossRef](#)]
43. Fu, W.; Hu, S.; Song, X.; Jin, C.; Li, J.; Zhao, Y.; Cao, J.; Wang, G. Effect of Ti content on the metallization layer and copper / alumina brazed joint. *Ceram. Int.* **2017**, *43*, 13206–13213. [[CrossRef](#)]
44. Lin, K.-L.; Singh, M.; Asthana, R. Characterization of yttria-stabilized-zirconia/stainless steel joint interfaces with gold-based interlayers for solid oxide fuel cell applications. *J. Eur. Ceram. Soc.* **2014**, *34*, 355–372. [[CrossRef](#)]

